Indian Journal of Engineering & Materials Sciences
Vol. 32, April 2025, pp. 198-210
DOI: 10.56042/ijems.v32i02.14491

Characteristics of acoustic emissions generated during the electrochemical corrosion process of steel reinforcement in reinforced concrete beams

Vidya Sagar Remalli[a]* & Anjali Purathekandy[a]

[a]Department of Civil Engineering, Indian Institute of Science, Bangalore 560 012, India

Received: 18 October 2024; accepted: 27 December 2024

This article reports the characteristics of acoustic emissions (AE) generated during the electrochemical corrosion process in reinforced concrete (RC) beam specimens. The RC beam specimens have been subjected to electrochemical corrosion in a NaCl solution container that has been present in the laboratory. The gaussian mixture modeling (GMM) algorithm has been employed to classify the AE generated during both the corrosion of steel rebar and the fracturing of concrete. A sudden increase in the generation of AE signals has been observed with the initiation of steel-rebar corrosion in the RC beam. The AE hits recorded during the initial stages have exhibited short durations of less than approximately 0.5 milliseconds. However, as corrosion has progressed, both the signal strength and the duration of the AE waveforms have increased. The extended monitoring duration has also affected the position of the knee in the cumulative AE signal strength (CSS) curve. The transition from micro-cracks to macro-cracks has been identified through the AE waveform parameter 'duration', which, in the later stages of accelerated corrosion, has ranged between 20 to 40 ms. The study reported in this article has been related to very accelerated corrosion, compared to an in-situ case where corrosion is much slower and likely environmental sources have dominated the total AE released. However, the findings of the present study may prove valuable for long-term monitoring of the corrosion process in RC structures.

Keywords: Acoustic emission, Chloride, Cumulative signal strength (CSS), Electrochemical corrosion, Gaussian mixture modeling, Reinforcement steel

1 Introduction

Reinforced concrete (RC) structures can handle tough weather and environmental conditions, making them suitable for long-term use in various construction applications[1]. However, structural failures can occur when the steel reinforcement in RC structures undergoes corrosion[2]. It is well known that this corrosion is an electrochemical process involving both electrical and chemical reactions[3].

1.1 Corrosion due to chloride

It is well established that the primary causes of steel rebar corrosion in RC structural components are the penetration of chloride ions (Cl^-) and carbon dioxide (CO_2) into the cementitious material. Steel reinforcement corrosion involves the movement of ions between areas of differing electrical potential on the surface of the reinforcement[2]. This ion transfer occurs through the pore solution within the concrete, which serves as the electrolyte. The steel reinforcement within concrete remains protected due to the high alkalinity of the surrounding layer[2,3]. This layer, composed of ferrous (Fe^{2+}) or ferric oxides, serves as a protective barrier that slows down or prevents further oxidation of the steel when exposed to moisture and oxygen[2,3]. The protective film remain stable unless disrupted by carbonation or chloride intrusion[2,3]. The chloride corrosion occurs more frequently with greater costs and effects on structural safety. Potential sources contributing to corrosion include aggregates, mix water, chemical admixtures, exposure to marine environments, and the use of anti-icing salts[3,4].

Over time, ferrous oxide (FeO) gradually transforms into the more stable ferric oxide. However, the conversion of ferrous oxide to ferric oxide is never entirely complete[3,4]. De-passivation of protective film occurs when the concentration of chlorides at the reinforcement surface surpasses a threshold value, generally ranging from 0.4% to 1% by mass of the binder[4]. Although some research exists, the detailed process of corrosion by Cl^- in concrete remains relatively insufficiently studied in the literature. The oxidation of steel reinforcement involves the following reaction:

$$Fe \rightarrow Fe^{2+} + 2e^- \quad \ldots(1)$$

*Corresponding author (Email: rvsagar@iisc.ac.in)

In most oxidation processes, oxygen typically acts as the oxidizing agent, meaning it accepts the electrons lost by the metal or other substances[4]. This electron transfer often results in the formation of oxides, such as:

$$4Fe + 3O_2 \rightarrow 2Fe_2O_3 \quad \ldots(2)$$

In the case of steel rebar corrosion, ferrous hydroxide [$Fe(OH)_2$] undergoes oxidation in the presence of oxygen and moisture, resulting in the formation of rust[4]. Specifically, iron (Fe) reacts with oxygen (O_2) to produce iron oxide (Fe_2O_3) commonly known as rust.

$$3Fe(OH)_2 \rightarrow Fe_3O_4 + H_2 + 2H_2O \quad \ldots(3)$$

The corrosion products that form tend to expand in volume, leading to further deterioration of the concrete. Chloride-induced corrosion occurs more rapidly and is characterized by pitting, a form of localized corrosion[3,4].

1.2 A brief literature review

Ahmad *et al.*[5] review the methods for monitoring corrosion damage and approaches for predicting service life. Bhaskar *et al.*[6] reviewed the studies on corrosion of rebars in RC structures. Song *et al.*[7] review focuses on the mechanisms of steel reinforcement corrosion in RC structures, along with assessment methods and corrosion control strategies. Researchers have primarily focused on investigating the corrosion in both conventional RC structures and externally wrapped RC structures[8-10]. Patil *et al.*[11] used the acoustic emission (AE) testing to evaluate and quantify rebar corrosion in RC structures. In addition, an experimental investigation was conducted to compare AE and electrochemical process for evaluating steel rebar corrosion in concrete[12]. The development of a quantitative method by establishing a nonlinear relationship between loss of mass and cumulative AE signal strength (CSS) was performed[12]. Several cylindrical specimens containing steel reinforcement were tested in the laboratory using 3% and 5% NaCl aqueous solutions under a constant potential of 5V. The results showed that the CSS exhibited a linear trend during the corrosion[13]. However, a noticeable shift in the CSS versus monitoring time curve was observed with the initiation of micro-cracking in the concrete[13]. The knee point in the CSS curve can serve as an indicator for the micro-cracks formation in concrete[14]. At the onset of crack nucleation, a relatively high burst of energy is released, which is reflected as a sudden increase or knee in the CSS curve[15]. Idrissi and Limam presented a correlation between AE activity evolution and corrosion process occurring within a reinforced concrete test specimen[16,17]. Benedetti *et al.*[18] investigated accelerated corrosion and offered valuable insights into the design of the corrosion circuit, the continuous monitoring procedure, and the appropriate settings for AE waveform parameters used in data collection. Ing *et al.*[19] explored to quantify the corrosion rate using the AE waveform parameter known as absolute energy. Also, researchers have attempted to study the steel rebar corrosion process using AE testing in RC structures and effectively monitored the corrosion process to identify the initiation of steel rebar corrosion[20-23]. The onset and development of corrosion in RC are significantly influenced by the properties of the interfacial transition zone (ITZ), which acts as a preferential pathway for aggressive agents due to its higher porosity and weaker microstructure[24].

Abouhussien *et al.*[25] used AE waveforms to evaluate the bond strength in corroded reinforced concrete beams. Van Steen *et al.*[26] represented a clustering algorithm that depends on the cross-correlation coefficient, which was applied to differentiate AE waveforms generated by various damage mechanisms during accelerated corrosion. The waveforms were grouped into two distinct clusters: the first cluster included signals associated with corrosion activity, hydration, moisture absorption, and microcracking, while the second cluster comprised waveforms resulting from macrocrack formation[26]. Further subdivision of the first cluster proved challenging due to the overlapping features of the AE signals.

Li *et al.*[8] monitored the accelerated corrosion process in steel-reinforced mortar blocks using both AE and fiber bragg grating (FBG) strain sensors[27]. While the FBG sensors detected expansion in the mortar, the AE testing was employed to track the development and propagation of cracks.

Ohtsu *et al.*[28] showed a phenomenological model to describe the corrosion in RC, illustrated in Fig. 1a[28]. This model divides the corrosion progression into four distinct phases. Phase 1 represents the initiation stage of corrosion. In Phase 2, corrosion loss begins to accelerate as corrosion products start to build up on the surface of reinforcement. Over time, this accumulation restricts the flow of oxygen, leading to a

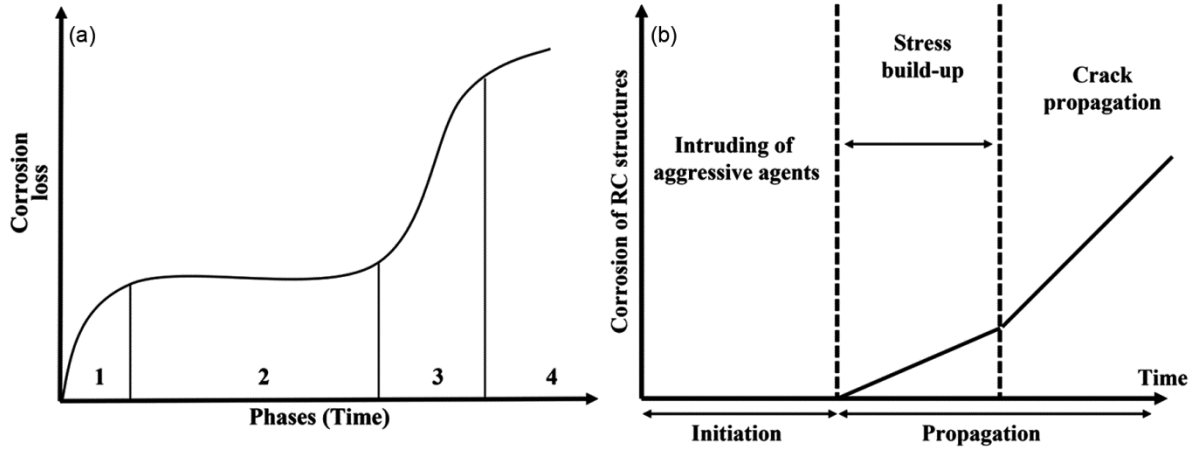

Fig. 1 — (a) A schematic illustration of the phenomenological model[9,28] & (b) Schematic illustration of typical service life model depicting reinforcement steel corrosion in RC structures, including cracking in steel and/or concrete[5,9,28].

gradual reduction in the corrosion rate by the end of this phase. Phases 3 and 4 represent anaerobic corrosion processes and follow patterns similar to those in Phases 1 and 2, respectively. As shown in Fig. 1b[28], many service life prediction models for RC structures prone to reinforcement corrosion are built around the first three phases of this framework.

Ohtsu *et al.*[28] also carried out accelerated corrosion experiments along with cyclic wet dry testing to investigate the corrosion behaviour of RC specimens under laboratory conditions using AE testing[28]. The observations showed that the AE activity aligned well with the stages described in the phenomenological corrosion model. The service life model is generally categorized into three phases. The first is the initiation phase, which refers to the time between the breakdown of the protective layer caused by chloride ingress or carbon dioxide penetration and the actual onset of corrosion[28]. This is followed by the stress build-up phase, where corrosion products begin to form and accumulate on the steel surface. The final phase is the rapid corrosion and deterioration phase, characterized by accelerated corrosion activity, significant crack growth, and spalling of the concrete cover[28].

1.3 Distinguishing AE waveform parameters for steel corrosion and concrete cracking

In RC structures, AE signals are produced during steel corrosion primarily due to two phenomena: (i) the corrosion activity occurring within the steel reinforcement, and (ii) the cracking or fracturing of the surrounding concrete affected by stresses generated from corrosion[29]. The AE signals produced by these two sources exhibits distinct characteristics. Because the AE waveform frequency is different when compared with AE waveform frequency from steel rebar[30]. Also, concrete is quasi-brittle material and steel rebar is a ductile behaviour under tensile loads. Cracking in concrete caused by the expansion of corroding reinforcement is primarily tensile in nature. As corrosion advances, more corrosion products accumulate, leading to increased internal pressure as a result of the restraining effect of the surrounding concrete[31,32]. This growing pressure influences the nature of the stress waves emitted. Notably, concrete cracking typically occurs only after the corrosion has reached a critical level. Therefore, the signals emitted have high AF ($\frac{Counts}{Duration}$) and low RA value ($\frac{Rise\ time}{Peak\ amplitude}$). Because the energy emissions generated during concrete fracture are burst type and the same generated from steel are continuous emissions. The signals emitted at the start of steel corrosion have high AF and low RA value like those emitted during tensile cracking[33]. But as the corrosion progresses, the AF value of the signals drop whereas RA value rises. The shift in signal characteristics can be linked to the gradual buildup of corrosion products. Since concrete has limited capacity to withstand tensile forces, these stresses eventually result in the formation of cracks[34,35].

Since cracking in concrete occurs only after the corrosion has reached an advanced stage, the AE waveforms recorded during the process naturally separates into two distinct clusters. The clusters represent: (i) AE signals generated by the corrosion of steel reinforcement, and (ii) AE signals resulting from cracking in the surrounding concrete. The gaussian mixture modeling (GMM) algorithm is effective in

classifying these two types of AE data[36,37]. Additionally, a method proposed in JCMS-III B5706[38] offers a way to monitor crack propagation in RC structures and classify the associated AE signals.

AE data are inherently random and often nonlinearly separable, making their classification challenging. Since the occurrence of AE events during the fracture of materials is unpredictable, it becomes important to consider the distribution characteristics of the AE waveform data for more accurate classification. A probabilistic approach, such as GMM, is well-suited for this task as it accounts for the underlying data distribution[36,37]. Using GMM, AE signals can be effectively grouped into two dominant categories: tensile and shear. The next section provides a brief overview of the GMM algorithm.

1.4 Theoretical background of GMM for AE signal analysis in corroding RC structures

GMM is a probabilistic clustering technique that assumes the data points originate from a combination of several multivariate normal distributions, each associated with a specific probability[36]. One of the key advantages of GMM is that it can group data into distinct clusters without prior knowledge of the actual category or label of any data point[36]. The clustering is performed using a soft assignment approach, where each data point is assigned to a cluster with a certain probability, rather than a hard classification. This process is carried out using the Expectation-Maximization (EM) algorithm. The probability density function (PDF) for a gaussian distribution is defined as[37]:

$$P(x|\mu,\sigma^2) = \frac{1}{\sqrt{2\pi\sigma^2}} e^{\left[\frac{-(x-\mu)^2}{2\sigma^2}\right]} \quad \ldots(4)$$

where μ represents mean and σ^2 is the variance, σ is the standard deviation, x is the single random variable.

In the present study, two gaussian components have been considered within the GMM framework[37]. These components represent two distinct sources of acoustic emission: one resulting from the corrosion process from the steel reinforcement, and the other from the fracture processes occurring in the surrounding concrete. The gaussian mixture model equation that governs this classification is presented in Eq. (5).

$$P(X|\mu,\Sigma) = \frac{1}{\sqrt{2\pi|\Sigma|}} e^{\frac{-1}{2}[(X-\mu)^T\Sigma^{-1}(X-\mu)]} \quad \ldots(5)$$

where, Σ denotes the covariance matrix of dimensions $n \times n$, μ represents the mean ($n \times 1$), n corresponds to the total number of data points, and X is the random variable ($n \times 1$). Further details are given in[36].

1.5 Motivation

AE testing for studying the cracking of RC due to corrosion in steel rebars has not been widely explored, and only limited detailed results are available in the literature. The corrosion is one of the causes of the failure, and must be studied and analyzed, so that the RC structural members may not develop unseen problems such as unexpected microcracking in reinforced concrete structural members which may lead to loss of aesthetics of the structure.

Most previous studies on monitoring the corrosion process in RC structures using AE testing have primarily focused on the early stages, particularly the initiation phase of corrosion. Also, several studies have been conducted by using AE testing for detecting electrochemical processes. But relatively few studies were reported on classification of AE waveforms generated due to (i) steel rebar corrosion and (ii) cementitious matrix cracking. Therefore, it becomes essential to classify the AE waveforms associated with two key phenomena: corrosion and microcracks initiation. This study presents a novel approach by utilizing GMM to interpret AE signals recorded during the accelerated corrosion of RC beams.

1.6 Aim of the study

The aim of this study is to evaluate how effectively AE testing can monitor the corrosion of steel reinforcement in RC beams exposed to a 3% NaCl solution. By applying the GMM algorithm, the AE signals recorded during the corrosion process were classified to distinguish between different sources of damage. All experimental investigations were carried out under accelerated corrosion conditions in the laboratory where AE waveforms were continuously recorded throughout the testing period.

2 Materials and Methods

2.1 Test specimens and materials

An accelerated corrosion testing (ACT) was performed on RC beams to investigate the corrosion behaviour of steel reinforcement and the resulting crack formation in concrete. The geometric specifications about the test specimens are given in Table 1. The materials used included ordinary portland cement (OPC) as per the requirements of IS:12269-1987, steel reinforcement bars of 8 mm and

Table 1 — Details of the RC beam specimens.

RC beam specimen	Dimensions (mm) Length X Depth X Breadth	Duration of accelerated corrosion (days)	Cross sectional area of steel bar (A_{st}), mm^2	Concentration of NaCl solution (%)
FF1	1000 X 200 X 120	5	100.57	3
FF2	1000 X 200 X 120	10	100.57	3
FF3	1000 X 200 X 120	15	100.57	3

12 mm diameters, coarse aggregates of 10 mm nominal size as coarse aggregate, and river sand classified under Zone-I as per IS:383-2002 for fine aggregate[39-41].

For each cubic meter of concrete, the mix was proportioned with 520 kg of cement, 894 kg of fine aggregate, and 825 kg of coarse aggregate. The mix was prepared with a water-to-cement ratio of 0.4 by weight. Three RC beam specimens labeled FF1, FF2, and FF3 were prepared, each having dimensions of 1000 mm in length, 120 mm in breadth, and 200 mm in depth. The concrete used in these specimens achieved a 28 day uniaxial compressive strength of 53 MPa. The design and detailing of the RC beams were carried out in accordance with the guidelines specified in IS 456:2000[42].

2.2 Accelerated corrosion test setup

Once the 28-day curing was complete, the RC beam specimens were removed from the curing setup. The specimens were placed under accelerated corrosion conditions within the laboratory environment. For this purpose, they were partially submerged in a sodium chloride (NaCl) solution with a concentration of 3% by weight. The solution was contained in a rectangular tank measuring 1300 mm in length, 1200 mm in width, and 350 mm in depth, which was used throughout the duration of the experiment. In the experimental setup, the steel reinforcement bars embedded in the RC beams were subjected to a constant direct current voltage of 5 volts. To establish the electrochemical circuit, a copper wire was used as the cathode, while the embedded steel rebar served as the anode. Accordingly, the positive terminal of the DC power supply was connected to the longitudinal reinforcement, and the negative terminal to the copper wire, initiating the accelerated corrosion process. To maintain reliable electrical connectivity during the corrosion process, small holes of 2 mm diameter were drilled into the longitudinal steel reinforcement bars. A connection was established to the power supply's positive terminal using the wires through these holes and fastening them securely. The setup used for the accelerated corrosion test to monitor corrosion in the steel rebars of RC beam specimens is shown in Fig. 2a. The reinforcement configuration within the RC beam is depicted in Fig. 2b.

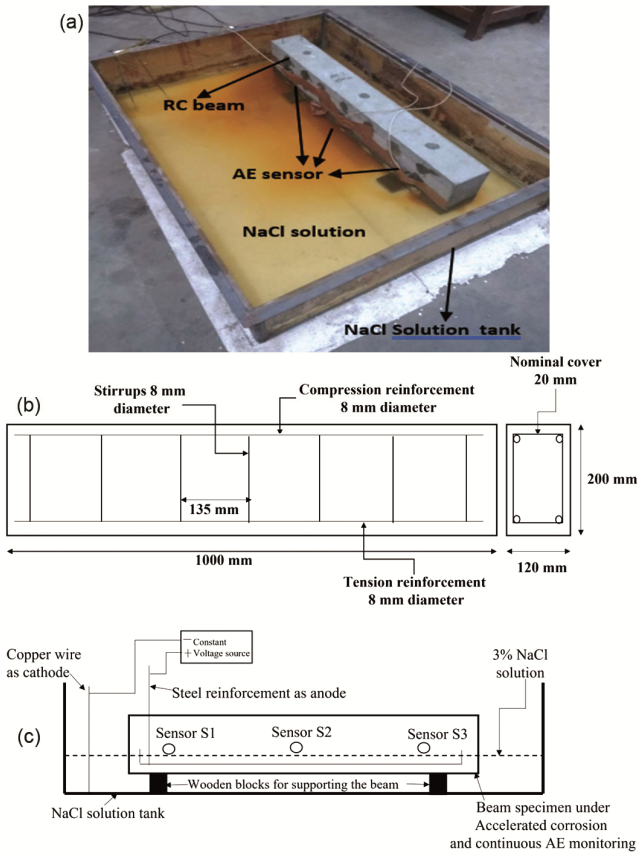

Fig. 2 — (a) Accelerated corrosion test arrangement, (b) Reinforcement detailing of test specimen and (c) Schematic representation of accelerated corrosion test setup and the depth dimension of the amount of beam in the NaCl solution is 50mm approximately.

2.3 AE recording setup

AE signals were recorded using an eight-channel AE recording system during the corrosion of steel reinforcement and cracking of concrete. The AE setup included resonant-type differential-ended sensors operating at 60 kHz, preamplifiers, and a data acquisition unit. These sensors were sensitive across a natural frequency of 54 kHz, with peak sensitivity at

75 dB, referenced to 1V/(m/s). Three AE sensors designated as S1, S2, and S3 were arranged linearly in a 2D planar setup, aligned parallel to the X-axis on the XY-plane. The positions on the RC beam specimen are illustrated in Fig. 2c. Specifically, the sensors were placed at coordinates: S1 at (200 mm, 25 mm), S2 at (500 mm, 25 mm), and S3 at (800 mm, 25 mm). The inter distance between the three sensors was 300 mm. To minimize background noise, the AE detection threshold was set at 40 dB_{AE}, which corresponds to 1 μV after amplification (with 0 dB_{AE} taken as reference). Once the electrical potential was applied, AE activity was monitored continuously throughout the testing period. The pre-amplifier gain was set at 40 dB. These acquisition settings remained constant throughout the duration of the experiments. AE waveforms were recorded over different durations for the three RC beam specimens: 5 days for FF1, 10 days for FF2, and 15 days for FF3, all subjected to accelerated corrosion. The monitoring process was concluded for each specimen once corrosion products visibly emerged from the steel–concrete interface. Due to experimental constraints, a two-dimensional linear sensor arrangement was adopted, positioned near the steel reinforcement bar.

3 Results and Discussion

The AE waveforms generated from corrosion and crack formation mechanisms exhibit distinct characteristics. Specifically, the signals associated with steel corrosion differ noticeably from those produced during the cracking and fracture of cement concrete. Because AE is a phenomenon in which strain energy accumulated in a solid is released because of fracture process and thus generated transient elastic stress waves[34,35]. Thus, cracking will be depending on the cohesive strength between the atoms of the deformable solid[34]. Therefore, the AE signals produced as a result of steel rebar corrosion and those generated from cracking in concrete exhibit distinctly different characteristics. These differences arise because the underlying mechanisms corrosion and fracture produce varying stress waveforms, leading to unique AE signatures for each type of damage.

Figure 3 (a & b) shows the total AE hits recorded for 5 days, and 15 days of corrosion monitoring period and can be observed that as the time increases the AE generation due to corrosion also increased. Figure 4 (a-c) shows the CSS and duration (in microseconds) with respect to corrosion monitored

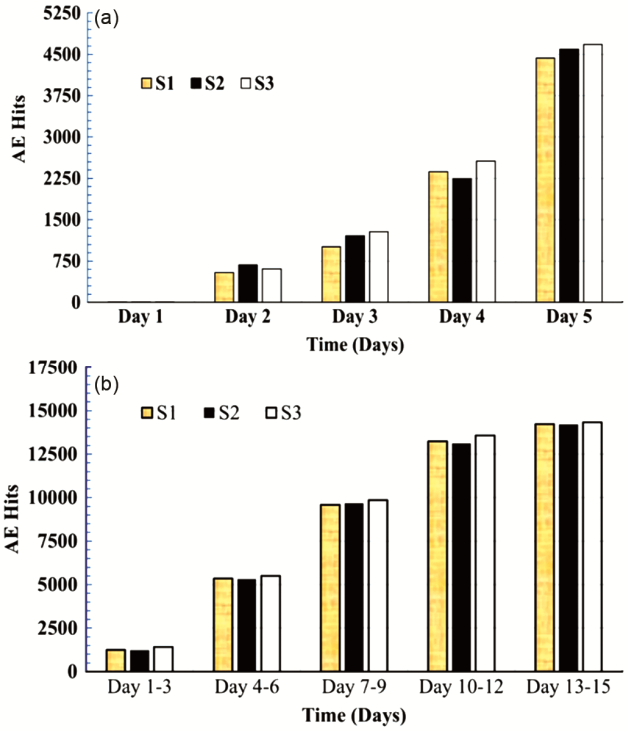

Fig. 3 — Total AE hits recorded during accelerated corrosion monitoring, (a) Specimen-FF1 and (b) Speicmen-FF2.

period and in the same figure the vertical dotted lines are where the steepness of the CSS curve changed. With the progression of the corrosion period, AE waves with higher signal strength were increasingly recorded. This indicates that as corrosion advances, the intensity and energy of the acoustic events tend to rise, reflecting more significant damage processes within the RC structure. From Fig. 4a, it is clear that multiple noticeable knees appear in the CSS curve, especially at the onset of corrosion. These knees are distinct and sharp, indicating sudden changes in AE activity. As time advances, the corrosion becomes more pronounced as seen in Fig. 4c, the height of these knees gradually decreases, showing a reduction in the intensity of AE events. Initially the CSS curve seems steeper and as the time increases the slope also decreased gradually. Also, higher duration AE emissions were observed as the time of the corrosion increased. The duration of the AE hits recorded at 5th day of the corrosion process is relatively less when compared to the corrosion process at 10 days and 16 days. Lesser strain energy may be released at 5th day when compared to the strain energy released at 10^{th} day and 16^{th} day.

The first noticeable knee in the CSS curve appears after two days, which corresponds with a rise in the

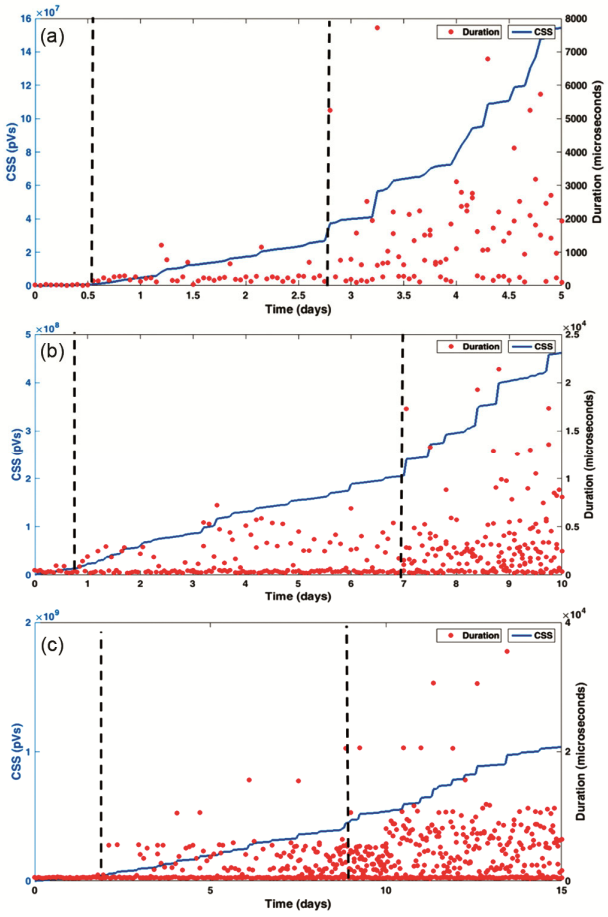

Fig. 4 — Variation of cumulative signal strength and variation of duration of all recorded AE hits for (a) Beam FF1, (b) Beam FF2 and (c) Beam FF3 (the vertical dotted lines are where the slope of the CSS curve changed).

duration of AE waveforms. This change likely signals the onset of micro-cracking within the concrete. Following this point, additional knees are observed in the CSS curve, indicating the continued formation of micro-cracks. The associated AE events also show increased durations, suggesting progressive damage within the structure.

In Fig. 4c, the knee in the CSS curve is not clearly visible due to the graph's scale limitations. This makes it difficult to identify changes in AE activity, highlighting the need for alternative methods to better distinguish the recorded AE hit data. Additionally, the pattern of CSS variation over time in Fig. 4 differs from the AE activity typically observed during active corrosion. Active corrosion progression is shown in Fig. 5. Figures 4(a-c) specifically present the variation of CSS for RC beams FF1, FF2, and FF3, subjected to accelerated corrosion for 5, 10, and 15 days, respectively. Active corrosion typically initiates in the steel reinforcement bars. This observation further supports the effectiveness of the CSS parameter in AE testing for detecting corrosion activity in steel rebars. The AE events recorded during the corrosion process are illustrated in Figs (5 – 7). For better visibility, the source locations in these figures have been slightly offset by 20 mm, ensuring that they are not obscured by the black circles representing the sensor positions.

It can be observed that as the corrosion progressed further the number of AE events increased more. The AE events were recorded in day - 1 as well as day - 2. It is because, during the initial period of accelerated corrosion, there might be noise in AE data generated due to the diffusion of salt solution and movement of trapped air bubbles inside the concrete void spaces[11-13]. These are also recorded as events and therefore the events generated during this period will be mainly attributed to these phenomena. This can also be confirmed from the AE CSS versus time and duration versus time plot shown in Fig. 4(a – c). For the first 12 hours, the AE hits recorded are of very low duration as shown in Fig. 4a. This corresponds to the de-passivation of the steel rebar. However, a noticeable increase in the duration of AE hits is observed after 12 hours, which suggests the onset of the corrosion process in the steel bar.

Figure 8 presents the cumulative AE hits recorded for the three RC beams over different corrosion monitoring durations. Longer exposure to corrosion environment resulted in more AE signals being recorded thus, more hits were observed. For example, beam FF1, which was monitored for 5 days, recorded approximately 14,500 AE hits. In contrast, beam FF3, monitored for 15 days, exhibited a significantly higher number of hits around 44,500. This clear increase in AE activity indicates that the corrosion process in the RC beams intensified over time.

To analyze the AE hit data generated during this process, the recorded AE hits were classified using the GMM algorithm. Two key waveform parameters were used for this classification: AF, defined as counts per duration, and RA value, defined as the ratio of rise time to peak amplitude. Figures (9 – 13) show the results of the GMM classification for specimen FF1, based on all recorded AE hits. In these figures, AE waveform amplitudes are represented on a decibel (dB) scale. The amplitude values shown are post-amplification readings, with 0 dB_{AE} corresponding to 1 μV at the sensor output (not after the preamplifier). While AE monitoring began on the

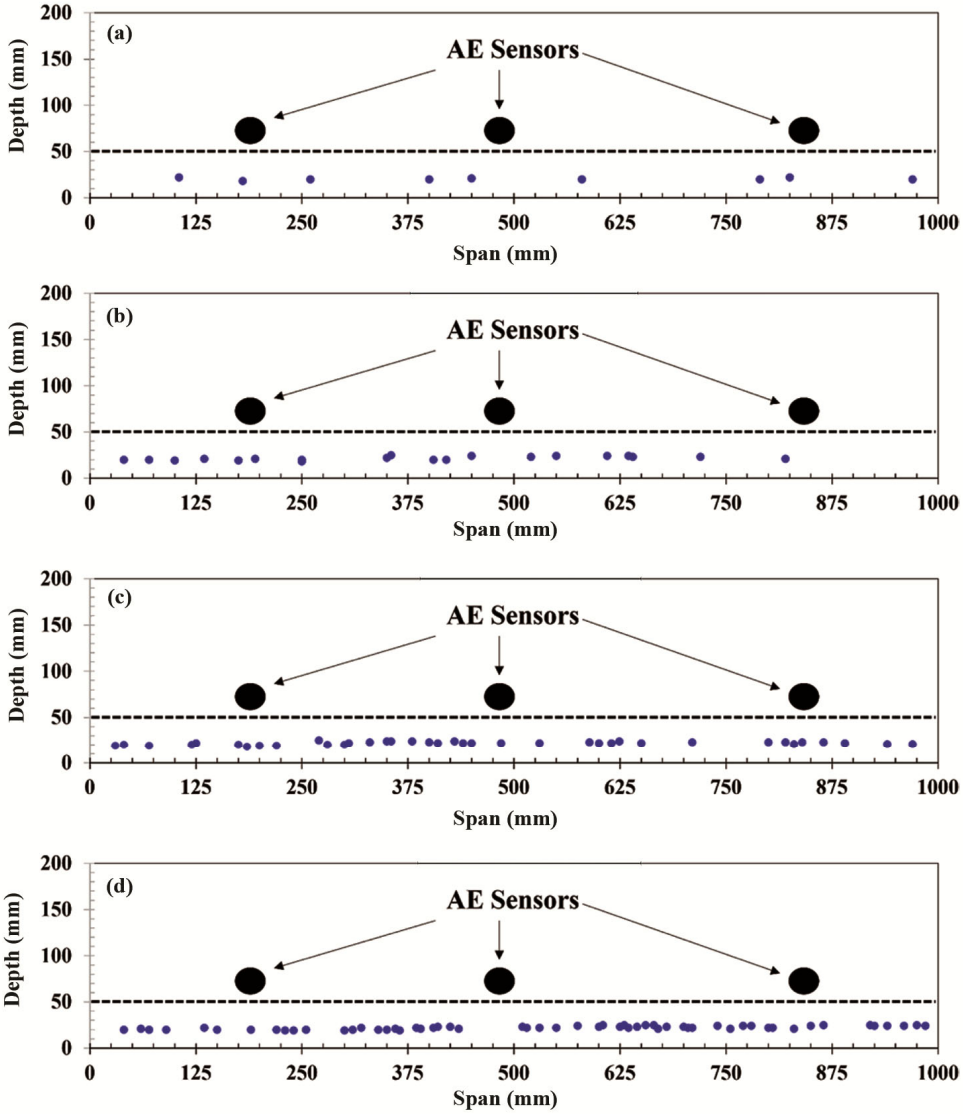

Fig. 5 — AE events location on day (a) 2, (b) 3, (c) 4 and (d) 5 observed using specimen - FF1. (*X- axis is span of the RC beam specimen; Y- axis is depth of the RC beam specimen, dashed line represents the top of the NaCl solution in the tank).*

first day of testing, the amount of AE hits recorded during that period was minimal. On day 2 of monitoring, the recorded AE data was categorized into two clusters using the GMM algorithm.

During this period, the primary activity influencing AE generation was the de-passivation and initial corrosion of the steel reinforcement. However, starting from Day 3, a new and distinct cluster began to emerge in the AE data. This additional cluster corresponds to the micro-cracks initiation within the concrete. As corrosion progressed into Day 3 and Day 4, the distinction between these two clusters became more evident. The 3D GMM plots presented in Figs (11 & 12) clearly show the separation of AE signals associated with corrosion in steel and cracking in concrete. At the initial stage of corrosion, the AE signals generated typically exhibit high AF and low RA values. This behaviour is comparable to AE patterns seen during tensile and shear cracking under mechanical loading in solid materials. However, as the corrosion process advances, there is a noticeable shift in AE signal characteristics AF values tend to decrease while RA values increase. This transformation in waveform parameters is likely due to the gradual accumulation of build-up of oxidized compounds on the steel bars, which alters the stress distribution and fracture behaviour. As shown in Fig. 14, the early phase of corrosion is

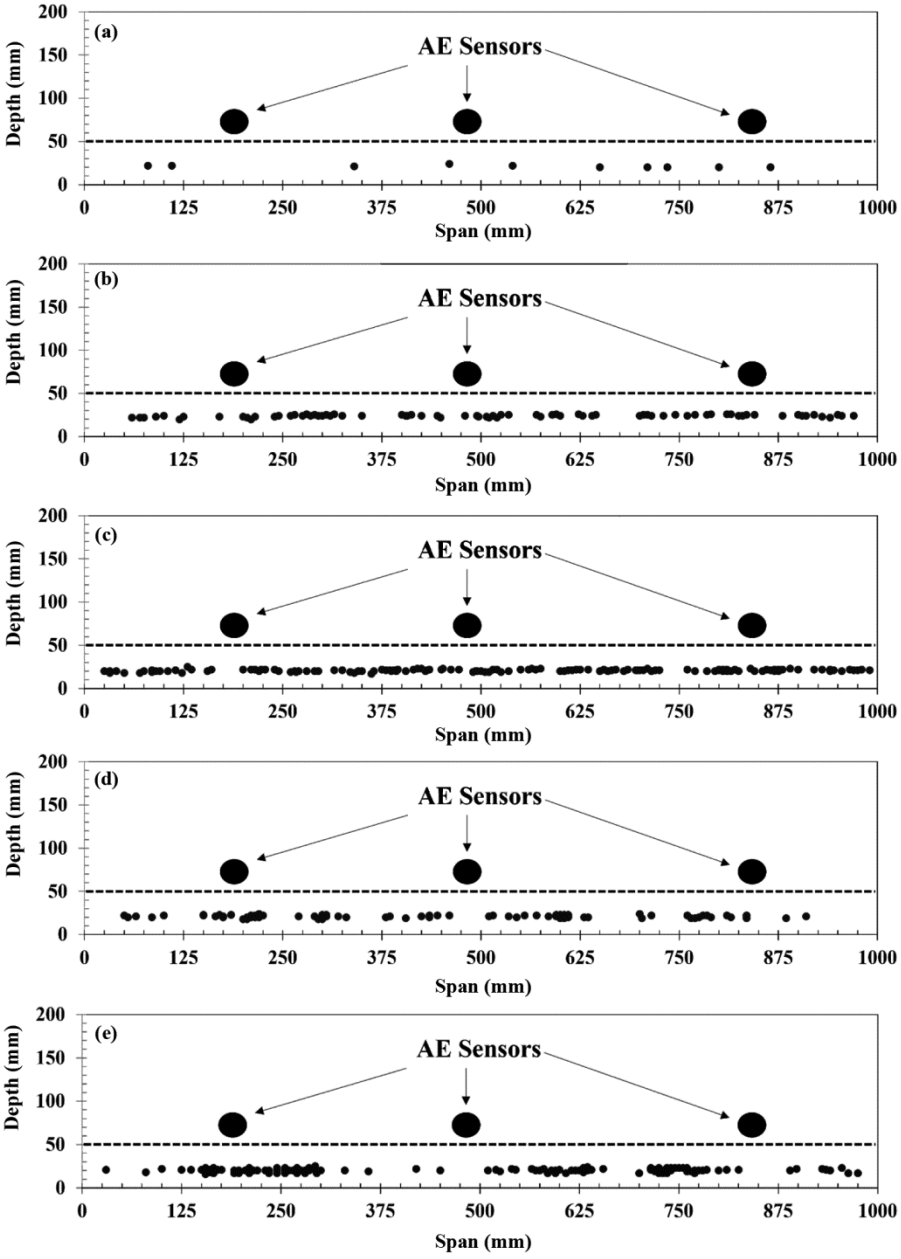

Fig. 6 — AE events location on days (a) 1-2, (b) 3-4, (c) 5-6 (d) 7-8 and (e) 9-10 observed using specimen - FF2. *(X-axis is span (mm) of the RC beam specimen; Y-axis is depth (mm) of the RC beam specimen, dashed line represents the top surface of the NaCl solution in the tank).*

marked by a rise in AE hit count, a reduction in RA values, and an increase in AF, signaling the active onset of the corrosion process.

3.1 Practical significance

Steel rebar corrosion poses a greater threat to in-situ RC constructions found in coastal regions. It is beneficial to conduct AE testing to track the fracture process in these RC structures. The period of time between the de-passivation of the protective coating on the steel bars' surface due to CO_2 penetration or chloride attack is known as the corrosion beginning phase. Following the start of corrosion, the stress build-up phase involves the production and formation of corrosion by products on embedded steel. During this stage, the concrete experiences hoop stresses brought on by the expansive pressure created by the steel-concrete interface's controlled expansion, which causes longitudinal cracks to start. A phase of fast corrosion and deterioration follows, characterised by

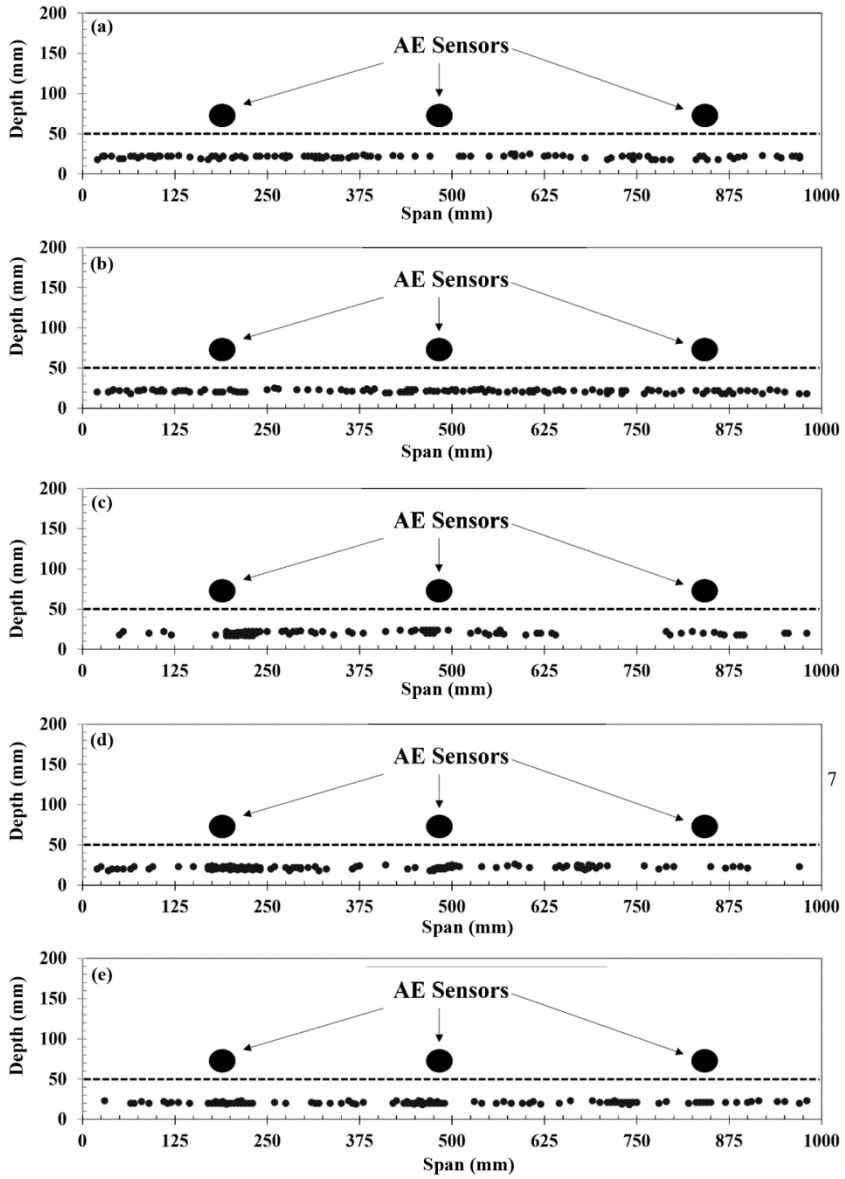

Fig. 7 — AE events location on days (a) 1-3, (b) 4-6, (c) 7-9 (d) 10-12 and (e) 13-15 observed using specimen – FF3. (*X- axis is span (mm) of the RC beam specimen; Y- axis is depth (mm) of the RC beam specimen*, dashed line represents the top of the NaCl solution in the tank).

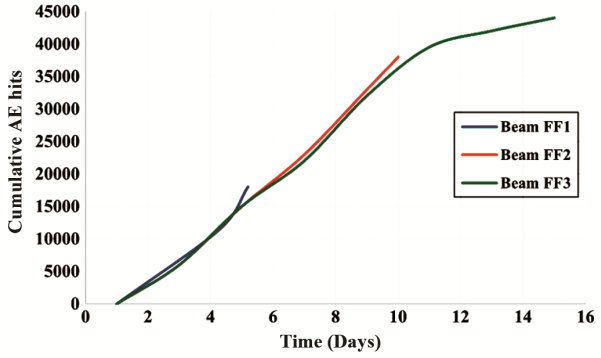

Fig. 8 — Cumulative AE hits recorded with time for the three RC beams.

the spalling of cover concrete and the rapid formation of cracks.

Certainly, there is difference between AE recorded in a RC beam specimen under accelerated corrosion in laboratory and the AE recorded in-situ RC structures which are under corrosion process. AE during non-accelerated corrosion in real RC structures will have a large amount of extraneous AE, hence there is a need to eliminate the extraneous noise by setting appropriate AE detection threshold. Also, the AE from corrosion aspects will be spread out in time so may not be able to identify "knees" as observed during laboratory experiments.

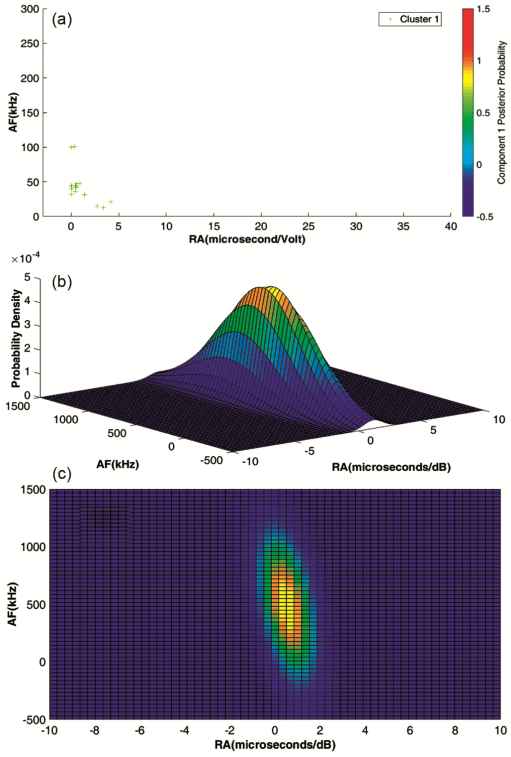

Fig. 9 — Beam FF1-Day 1 plots (a) AF versus RA plot with component posterior probability, (b) 3D-GMM plot of corrosion data and (c) 2D-GMM plot of corrosion data.

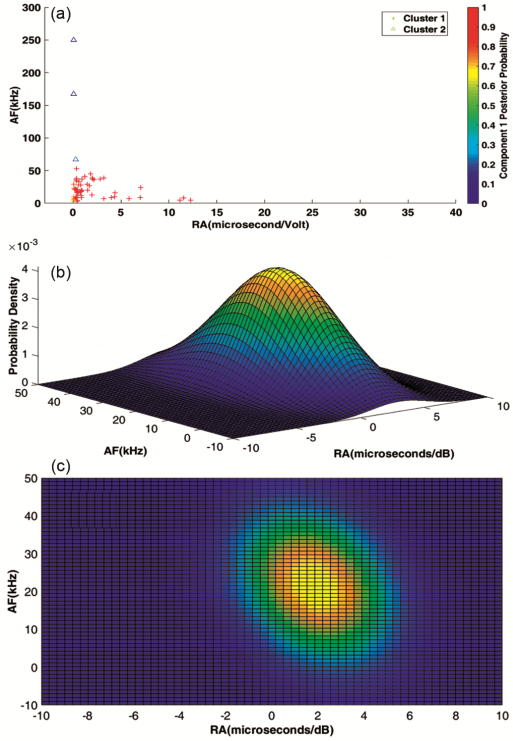

Fig. 10 — Beam FF1-Day 2 plots (a) AF versus RA plot with component posterior probability, (b) 3D-GMM plot of corrosion data and (c) 2D-GMM plot of corrosion.

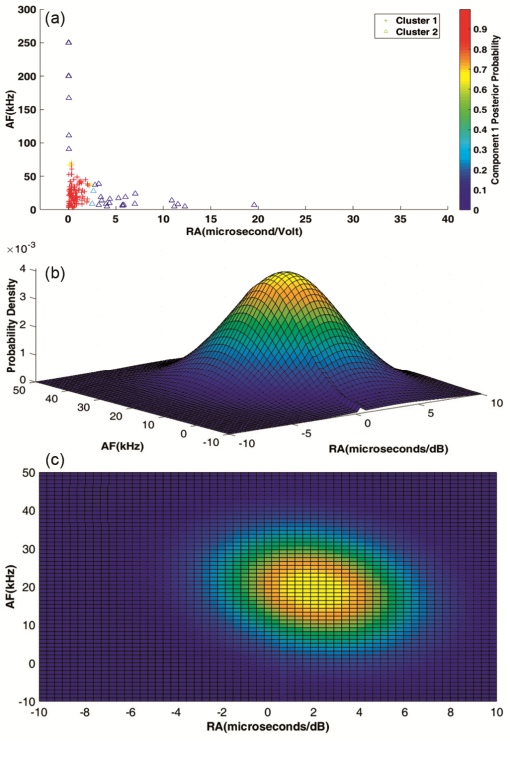

Fig. 11 — Beam FF1-Day 3 plots (a) AF versus RA plot with component posterior probability, (b) 3D-GMM plot of corrosion data and (c) 2D-GMM plot of corrosion data.

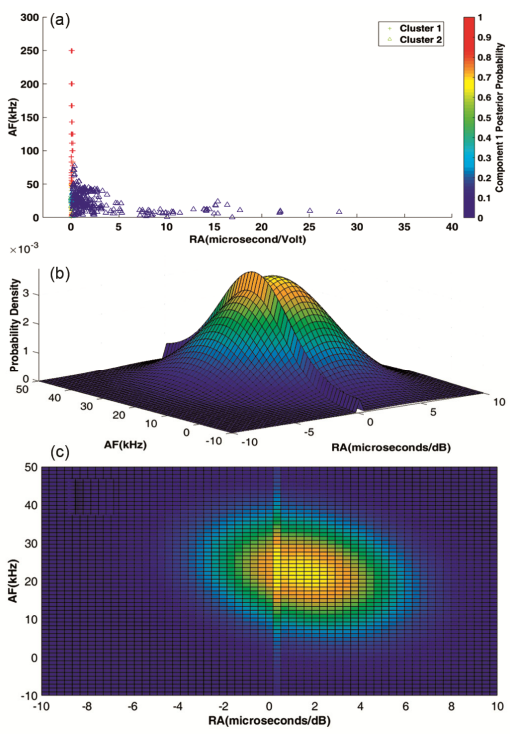

Fig. 12 — Beam FF1-Day 4plots (a) AF versus RA plot with component posterior probability, (b) 3D-GMM plot of corrosion data and (c) 2D-GMM plot of corrosion data.

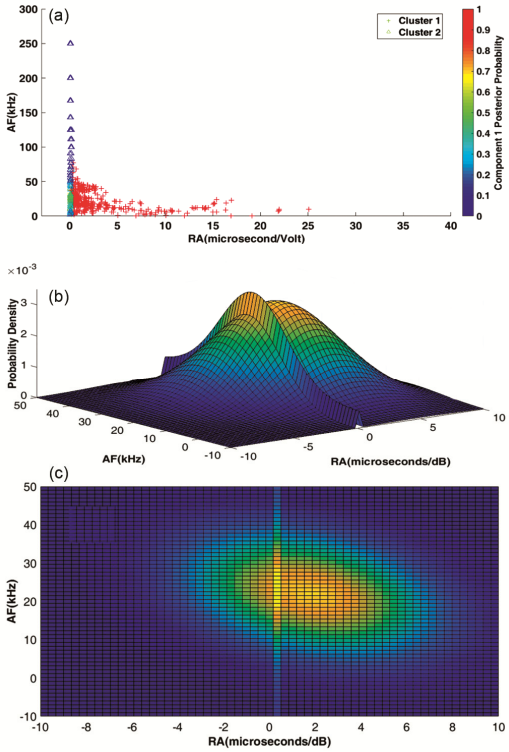

Fig. 13 — Beam FF1-Day 5 plots (a) AF versus RA plot with component posterior probability, (b) 3D-GMM plot of corrosion data and (c) 2D-GMM plot of corrosion data.

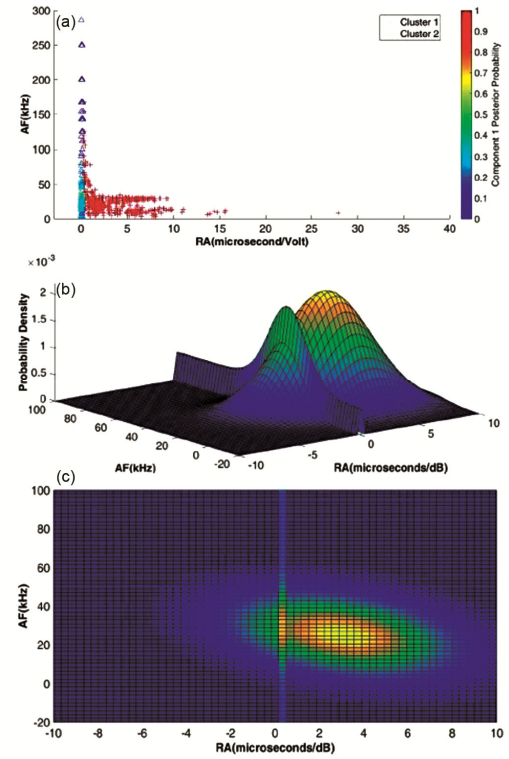

Fig. 14 — Beam FF3-Day 7 – Day 9 plots (a) AF versus RA plot with component posterior probability, (b) 3D-GMM plot of corrosion data and (c) 2D-GMM plot of corrosion data.

In the present study authors did not obtain waveforms in their experiments, only the AE waveform parameters were recorded. Certainly, there will be an influence of cement concrete mixture composition on AE hits signal parameters. The present study is an attempt to implement AE testing on corrosion process in RC structures. The study is limited to focusing on characteristics of AE generated during the electrochemical corrosion of steel rebar in RC beams. Classification of AE generated from concrete cracking and corrosion in steel is very important and certainly authors are focusing in the future studies and machine learning concepts may be a suitable tool classify the AE generated during concrete cracking and steel rebar corrosion.

4 Conclusion

Based on the above experimental observation, the following conclusions are drawn:

a. A noticeable surge in the generation of AE waveforms was observed with the initiation of corrosion in the steel reinforcement within the concrete. Key AE waveform parameters such as signal strength, duration, RA value (rise angle), and average frequency (AF) proved valuable in tracking the progression of corrosion and identifying the development of cracks in the concrete. Among these, the variation in cumulative signal strength (CSS) emerged as a particularly effective indicator for monitoring corrosion in reinforced concrete structures exposed to accelerated corrosion conditions.

b. The AE hits recorded during the initial stages have a small duration of less than 0.5 ms. But with the progression of corrosion in steel rebar there was an increase in the duration of AE hits recorded. This increase in duration also corresponds with the knee in CSS curve. The evolution of micro cracks to macro cracks could be identified from the increased duration of AE hits recorded in the later stages of accelerated corrosion (20 ms to 40 ms).

c. The sensitivity of the CSS curve in identifying the cracking of concrete is dependent upon the environmental conditions.

d. Gaussian mixture modeling applied to the RA and AF values was observed to be effective in identifying the cracking in concrete. Two distinct peaks were observed in 3D GMM plots corresponding to concrete cracking and rebar corrosion as the corrosion progresses. Thus,

GMM could serve as an effective tool to study the progression of corrosion and identify cracking in concrete using AE waveform parameters.

e. At the early stage of accelerated corrosion, the steel reinforcement was found to corrode uniformly. As a result, AE were recorded all along the length of the bar. But in the later stages, localized corrosion was observed to occur. AE events recorded were clusters corresponding to localized corrosion and macro-cracks generation. Further experiments are required to confirm the above conclusions.

References

1 Verstrynge E, Van Steen C, Vandecruys E & Wevers M, *Constr Build Mater*, 349 (2022) 128732.
2 Brian B H, John A P & Alan K C, *Cem Concr Res*, 16(5) (1986) 771.
3 Gadve S, Mukherjee A & Malhotra S N, *Constr Build Mater*, 23 (2009) 153.
4 Zaki A, Chai H K, Aggelis D G & Alver N, *Sensors*, 15 (2015) 19069.
5 Ahmad S, *Cem Conc Comp*, 25(4-5) (2003) 459.
6 Bhaskar S, Bharatkumar B H & Gettu R, *Ind Conc J*, 12(3) (2011) 35.
7 Song H W & Saraswathy V, *Int J Electrochem Sci*, 2(1) (2007) 1.
8 Li Q, Melchers R E & Zheng J J, *ACI Str J*, 103(4) (2006) 479.
9 Kawasaki Y, Tomoda Y & Ohtsu M, *Constr Build Mat*, 24(12) (2010) 2353.
10 Ghods A, Sohrabi M & Miri M, *Mat Tehnol*, 48(3) (2014) 395.
11 Patil S, Karkare B & Goyal S, *Curr Sci*, 109(5) (2015) 943.
12 Patil S, Karkar B & Goyal S, *Constr Build Mater*, 68 (2014) 326.
13 Patil S, Karkare B & Goyal S, *Constr Build Mater*, 156 (2017) 123.
14 Caré S & Raharinaivo A, *Cem Concr Res*, 37 (2007) 1598.
15 Yuan Y, Ji Y & Shah S P, *ACI Struct J*, 104(3) (2007) 344.
16 Idrissi H & Limam A, *J Acou Emiss*, 18 (2000) 307.
17 Idrissi H & Limam A, *NDT & E Int*, 36(8) (2003) 563.
18 Di Benedetti M, Loreto F M & Nanni A, *J Mat Civ Eng*, 25(8) (2013) 1022.
19 Ing M, Austin S & Lyons R, *Cem Concr Res*, 35 (2005) 284.
20 Yoon D J, Weiss W J & Shah S P, *J Eng Mech*, 126(3) (2000) 273.
21 Kawasaki Y, Wakuda T, Kobarai T & Ohtsu M, *Constr Build Mater*, 48 (2013) 1240.
22 Dunn S E, Young J D, Hart W H & Brown R P, *Corr*, 40 (1984) 339.
23 Anjali P & Vidya Sagar R, "Characteristics of Acoustic Emissions Generated During Steel Rebar Corrosion in Reinforced Concrete", in Mukhopadhyay C K & Mulaveesala R (eds.), *Advances in Non-destructive Evaluation*, Lecture Notes in Mechanical Engineering, Springer, Singapore (2021) pp. 271–281.
24 Bhaskar S, Ravindra G & Bharat Kumar B H, *Ind conc J*, 91(3) (2017) 37.
25 A.A. Abouhussien, and A.A.A. Hassan. (2018). Acoustic emission monitoring of corrosion damage propagation in large-scale reinforced concrete beams. J. of Perf. of Const. Fac. 32(2): p. 04017133.
26 Van Steen C & Verstrynge E, *Appl Sci*, 12(4) (2022) 2154.
27 Li W, Xu C, Ho S C M, Wang B & Song G, *Sensors*, 17 (2017) 657.
28 Ohtsu M & Tomoda Y, *ACI Mat J*, 105(2) (2008) 194.
29 Pollock A A, *AE Signal Features: Energy, Signal Strength, Absolute Energy and RMS*, Acoustic Emission Tech Notes, Mistras Group Inc., 2014.
30 Tamer A, Maaddawy E & Soudki K, *J Mat Civ Eng*, 15(1) (2003) 41.
31 Aggelis D G, *Mech Res Commun*, 38(3) (2011) 153.
32 Ohno K & Ohtsu M, *Constr Build Mater*, 24(12) (2010) 2339.
33 RILEM Technical Committee, *Mat Str*, 43 (2010) 1187.
34 Grosse C U & Ohtsu M, Acoustic Emission Testing (Springer-Verlag, Berlin, Heidelberg), 4th Edn, ISBN: 9783540771216, 2008.
35 Malhotra V M & Carino N J, Handbook on Nondestructive Testing of Concrete (CRC Press, Boca Raton, FL, USA), 2nd Edn, ISBN: 9780849314859, 2004.
36 Farhidzadeh A, Salamone S & Singla P A, *Int J Mat Str*, 24 (2013) 1722.
37 Kottegoda N T & Rosso R, *Statistics, Probability, and Reliability for Civil and Environmental Engineers*, McGraw Hill International Edn, Singapore (1998).
38 JCMS-IIIB, *Monitoring Method for Active Cracks in Concrete by Acoustic Emission*, Federation of Construction Materials Industries, Japan (2003) 23.
39 IS: 12269-1987, *Specification for 53 grade Ordinary Portland Cement*, Bureau of Indian Standards, New Delhi (1987).
40 IS: 383-2002, *Specification for coarse and fine aggregates from natural sources for concrete*, Bureau of Indian Standards, New Delhi (2002).
41 ASTM G1-03, *Standard practice for preparing, cleaning, and evaluating corrosion test specimens*, ASTM Special Technical Publication, Pennsylvania, USA (1985).
42 IS 456-2000, *Plain and Reinforced Concrete - Code of Practice*, Bureau of Indian Standards, New Delhi (2000).